Journal of Computational Neuroscience 10, 151–172, 2001

Processing of Auditory Midbrain Interspike Intervals by Model Neurons

NATHAN R. WILSON AND DEANA A. BODNAR
Department of Neurobiology and Behavior, Cornell University, Ithaca, New York, USA
nathan1@mit.edu

JOSEPH F. SKOVIRA
IBM Corporation, Armonk, New York, USA

BRUCE R. LAND
Department of Neurobiology and Behavior, Cornell University, Ithaca, New York, USA

Received February 23, 2000; Revised August 22, 2000; Accepted September 22, 2000

Action Editor: S. Shamma

Abstract. A question central to sensory processing is how signal information is encoded and processed by single neurons. Stimulus features can be represented through rate coding (via firing rate), temporal coding (via firing synchronization to temporal periodicities), or temporal encoding (via intricate patterns of spike trains). Of the three, examples of temporal encoding are the least documented. One region in which temporal encoding is currently being explored is the auditory midbrain. Midbrain neurons in the plainfin midshipman generate different interspike interval (ISI) distributions depending on the frequencies of the concurrent vocal signals. However, these distributions differ only along certain lengths of ISIs, so that any neurons trying to distinguish the distributions would have to respond selectively to specific ISI ranges. We used this empirical observation as a realistic challenge with which to explore the plausibility of ISI-tuned neurons that could validate this form of temporal encoding. The resulting modeled cells—point neurons optimized through multidimensional searching—were successfully tuned to discriminate patterns in specific ranges of ISIs. Achieving this task, particularly with simplified neurons, strengthens the credibility of ISI coding in the brain and lends credence to its role in auditory processing.

Keywords: temporal coding, interspike intervals, model neuron, high-dimensional parameter optimization, auditory midbrain

1. Introduction

A fundamental question in neural function is how sensory information, such as sound frequencies or visual motion, are encoded and processed. A prevailing explanation is that of *rate coding*, in which the signal is directly encoded by the neuron's average firing rate, and any variability in that firing rate is considered noise. Since such noise can be filtered out by averaging across time or across populations, rate coding provides for a robust representation. Another form that a spike train may assume is summarized by the term *temporal coding*, which maintains that neurons can propagate information via synchronization of spikes to a stimulus's temporal periodicities. An alternate strategy to both rate coding and temporal coding is temporal *en*coding, which proposes that information is represented within the more intricate timing patterns of action potentials (Theunissen and Miller, 1995). Since a spike train can contain multiple temporal patterns,

temporal encoding potentially provides an efficient and information-rich representation. Empirically, temporal patterns in sensory systems such as vision (Richmond et al., 1990; McClurkin et al., 1991), touch (Ghazanfar et al., 2000), audition (Middlebrooks et al., 1994), and olfaction (Laurent et al., 1996; Wehr and Laurent, 1996) have been shown to convey information that firing rate and simple temporal coding do not.

The present study examines a candidate for temporal encoding in the auditory midbrain of the plainfin midshipman (*Porichthys notatus*), a teleost fish with an auditory system homologous to mammals (Palmer, 1990; Fay, 1993). Male midshipman produce low-frequency hums to attract passing females into their nests (Ibara et al., 1983; Brantley and Bass, 1994), and phonotaxis experiments (McKibben and Bass, 1998) have shown that female midshipman consistently prefer some calls over others, based in part on frequency. While the fish therefore has a demonstrated ability to encode frequency information, the mechanisms by which this information is propagated through the auditory pathways toward identification remain unknown.

The midshipman auditory system follows the same progression of frequency coding as that observed in other vertebrates including mammals. While afferents in the eighth nerve transduce frequency via synchronization (McKibben and Bass, 1999), his temporal code breaks down by the time it reaches the midbrain (Bodnar and Bass, 1997). Yet evidence for the temporal encoding of frequency information has been identified (Bodnar and Bass, 1999). By examining the first-order interspike intervals (ISIs) of spike bursts occurring within the beat periods of two-tone stimuli, they found that different sound frequencies generated different interspike interval distributions (Fig. 1). Specifically, pairs of two-tone beat stimuli were applied that shared a common difference frequency (dF) but differed in their frequency components (Fig. 1A). Spike trains from over a hundred neurons were recorded (Fig. 1B), whereupon the interspike intervals were measured and tabulated in histograms (Fig. 1C). Different ISI distributions in response to beats differing in their frequency components were generated by 97% of observed neurons. However, the distributions rarely seemed to differ across the entire range of ISIs; rather the frequency information was encoded in a narrow subrange of ISIs (Fig. 1D). For example, if two ISI distributions varied in length from 0 ms to 80 ms (Fig. 1C), they might be dissimilar with respect to ISIs of lengths 20 ms through 40 ms (Range *Y* in Fig. 1D). Since the two stimuli in each pair were controlled for dF, amplitude, and starting phase while only one frequency was varied, the significant differences found in the firing patterns could be construed to encode frequency information.

If this is indeed the case and frequency information is passed along subranges of available ISI bandwidth, the reception of this information would require cells that were selectively tuned to the same subranges (Fig. 1E). Thus an initial question into the plausibility of the code is whether standard nerve cells can attain this seemingly complex capability. Simple model neurons presented here demonstrate that they can and illustrate some of the properties that provide this faculty.

The model's success in this task, discussed below, provides two contributions. First, since the information contained in the recorded spike trains seems to pertain to frequency, the model provides an existence proof for how that information can be decoded and made available in higher auditory regions. Since no such information pertaining to fish is currently available, this is an important consideration. And as fish share qualitative abilities for the perception of complex sounds with other vertebrates (Fay, 1995) and are equipped with a homologous auditory anatomy (Popper and Fay, 1993), such lines of inquiry are most likely relevant to other vertebrates as well. Second, since the model is derived from an empirical scenario, it complements recent studies (i.e., Reich et al., 2000) exploring how neural architectures might be equipped to process interspike interval codes. This in turn lends understanding to a novel form of temporal encoding that is only now beginning to be acknowledged and explored.

2. Methods

2.1. Overview of Model Neurons

Nerve cells were modeled with the intent of developing neurons capable of responding selectively to narrow ranges of first-order interspike intervals. For an efficient approach, neurons were simulated through a 10 parameter point neuron model. The point neuron is an integrate-and-fire model that approximates the input-output dynamics of a neuron with an equivalent circuit localized at a single point in space. This approach was chosen to relieve computational burden while maintaining the most salient features of processing.

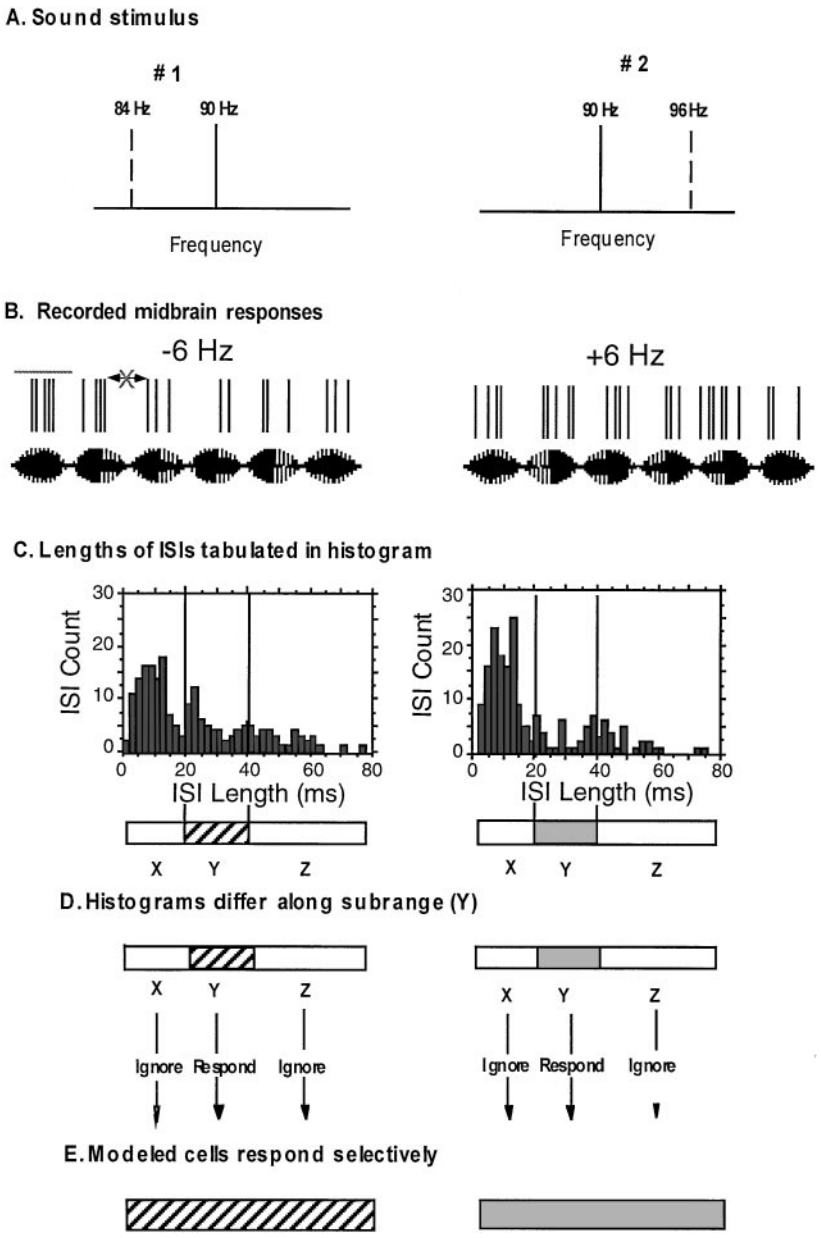

Figure 1. When different two-tone stimuli are presented to the midshipman fish, midbrain firings with different distributions of interspike intervals result. **A:** Two sound stimuli consisting of different tones are applied to a midshipman fish. Sound 1 consists of pure tones at 90 Hz and 84 Hz. Sound 2 consists of pure tones at 90 Hz and 96 Hz. **B:** Responses to these stimuli are recorded in the midshipman's midbrain. ISIs occurring within a beat cycle (indicated by the grey bar) were measured, while ISIs between beat cycles were excluded (grey X). **C:** Distances between the spikes in the recordings, or the interspike intervals (ISI's) are measured and recorded in a histogram. **D:** When the two histograms are compared, there is a range *Y* of ISI lengths across which the two histograms differ significantly. Elsewhere in the histogram, in ranges *X* and *Z*, the histograms are statistically similar (Bodnar and Bass, 1999). **E:** This motivates the present study of building model neurons that respond selectively to specific *Y* ranges, effectively selecting for specific ranges of interspike intervals.

Six parameters were allocated to represent somatic properties, while four parameters were used to model synaptic input.

2.2. Somatic Properties

Somatic properties were based on a standard MacGregor model (MacGregor, 1987), an integrate-and-fire framework that has successfully been applied to simulate systems from the network level (Balis et al., 1994) down to that of single auditory neurons (Ghoshal et al., 1992). The model was tuned to approximate an excitable membrane that, after crossing a threshold value, displays a rapid change in voltage followed by a rapid rectification period. The model was also made to show threshold accommodation to stimulation.

The state of the modeled cell is depicted by four state variables:

- S a binary variable that depicts whether the cell is firing or not,
- V the current voltage across the membrane of the cell,
- Th the current value of the threshold in mV (accommodation variable),
- gK the current level of potassium conductance (recovery variable).

We constructed a somatic model that relies on the balance between the forces of excitation, accommodation, and rectification. Each of these forces is dependent on two parameters, one which in a sense governs its rate and the other its magnitude.

2.2.1. Excitability

Initial Threshold Th_0. The initial threshold parameter Th_0 defines the membrane potential at which the cell exhibits an all-or-none response comparable to a Hodgkin-Huxley action potential. It was typically set from 10 to 20 mV above resting potential. As shown in Fig. 2, setting Th_0 to different values results in substantially different firing patterns.

Membrane Time Constant τ_m. The membrane time constant parameter τ_m determines the rate at which the membrane voltage V is depolarized by a stimulating current I, as exhibited by the following relationship:

$$\frac{dV}{dt} = -\frac{V}{\tau_m} + I.$$

The characteristic values for realistic firing ranged from 5 to 11 ms. Thus a shorter time constant meant for a more rapidly excitable membrane.

2.2.2. Threshold Accommodation. The threshold was allowed to accommodate to stimulation by moving above the initial threshold Th_0. This flexibility was added to provide the modeled cell with short-term plasticity. Hill (1936) popularized the use of accommodation through experimental validation in spinal motoneurons.

Threshold Sensitivity C. The amount by which the threshold accommodates per unit time is defined by the threshold sensitivity C. As exhibited in Fig. 3A, the threshold is more sensitive with larger values of C, which realistically varies from 0 to 1 (again, MacGregor, 1987).

Threshold Time Constant τ_{Th}. The threshold time constant τ_{Th} directly determines the rate of change in the threshold, with smaller values resulting in faster adjustment. Typical values selected ranged from 20 to 25 msec. All threshold accommodation variables were related in the model through the equation:

$$\frac{d(Th)}{dt} = \frac{-(Th - Th_0) + C * V}{\tau_{Th}}.$$

2.2.3. Rectification. Using simple parameters for potassium-driven rectification simulates Hodgkin-Huxley refractoriness. After an action potential, the potassium conductance exhibits a tail that extends until after the time necessary for excitation to return the membrane potential to resting level. An afterhyperpolarization of the membrane potential results, and the conductance further encourages refractoriness by leaking off excitatory current.

Potassium Conductance Strength B. The potassium conductance strength B (Fig. 3B) determines the magnitude with which the membrane repolarizes after firing a spike.

Potassium Conductance Time Constant τ_{gK}. τ_{gK} determines the length of the time course over which the rectification occurs. It is ranged from 3 to 10 msec, with smaller values conferring more rapid rectification (Fig. 3C).

In MacGregor's point neuron, the relationship between B and τ_{gK} is derived from an efficient model for rectification provided by Kernell (1968), incorporating

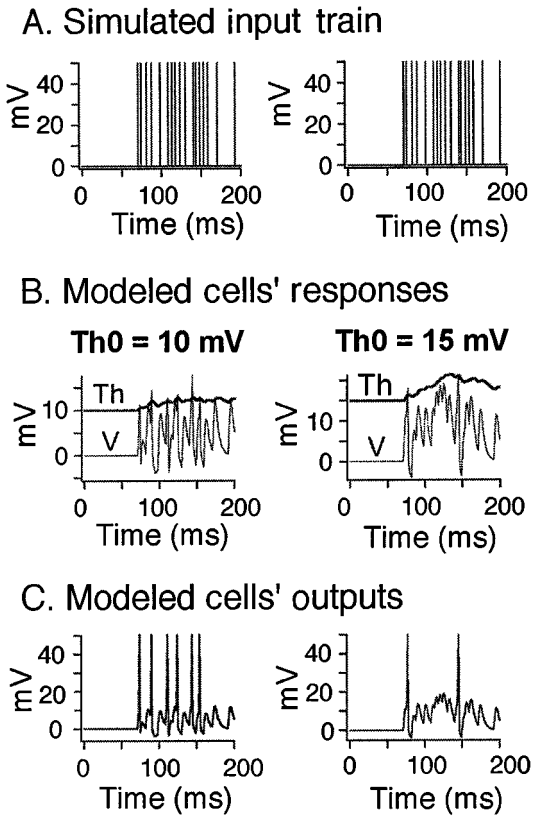

Figure 2. Setting for initial threshold Th_0 greatly affects the output of modeled cells. **A:** The same spike train is administered to two cells. **B:** One cell has an initial threshold set to 10 mV. The other is identical except that its initial threshold is set to 15 mV. **C:** Different firing patterns result from these different initial thresholds.

the spiking variable S:

$$\frac{d_g K}{dt} = \frac{-_g K + B * S}{\tau_{gK}}.$$

Altogether, while this model ignores the shape of the action potential, it does capture spike onset with the precise timing necessary for computation involving ISIs.

2.3. *Synaptic Properties*

Each synaptic pulse of current to the soma was represented by an attenuated four-parameter alpha function (see Jack et al., 1975). Synaptic impulses were initiated according to recorded spike times from the midbrain (see Section 2.5, Inputs to the Model, below). The shape of the pulse triggered at each recorded spike time was defined by the following function and parameters:

$$I = Y * \alpha^2 e^{-\alpha(xt)}(xt) \quad \text{where } t = 1 \ldots d.$$

2.3.1. Input Current Scale Y. Y (Fig. 3D) serves as the vertical scaling factor of the input function. It varies from 0 to 3, so that the synaptic current can be reduced down to near zero.

2.3.2. Input Time Constant α. α is a measure of the curvature of the synaptic function (Fig. 3E). It is possible for information to be conferred through the shape of the input current. Furthermore, it provides a curve that is more biologically plausible than the step function input that would otherwise result.

2.3.3. Input Time Scale x. x is the horizontal scaling parameter (Fig. 3F). Varying x, from 0.1 to 1, allows the curvature defined by alpha to be distributed differently across the multiple milliseconds for which each input spike acts.

2.3.4. Input Duration d. The entire alpha function is calculated over a range of t's determined by the spike duration. The usefulness of an intricate input

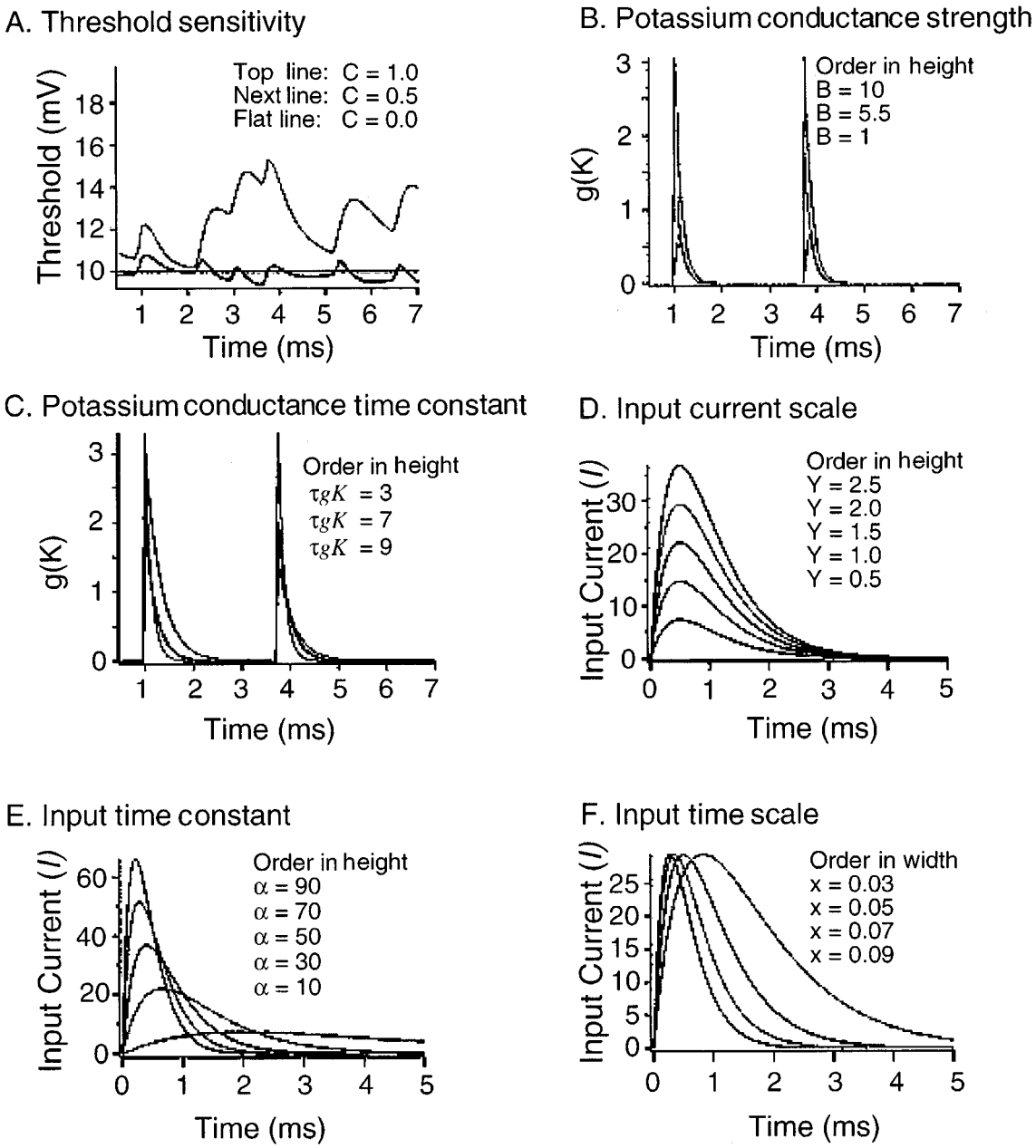

Figure 3. Varying the model's parameters affects its behavior in terms of certain state variables. **A:** Varying the threshold sensitivity C affects the position of the threshold. **B:** Varying the potassium conductance strength B modulates the overall potassium current in response to excitation. **C:** Changing the potassium conductance time constant $T_{g(K)}$ changes the time course of the potassium current. Larger values promote a longer current. **D:** The synaptic current can be scaled by changing the parameter Y. **E:** The parameter α allows control over the curvature of the synaptic input function. **F:** A given synaptic input function can be stretched horizontally by varying the parameter x.

function is to provide the cells with the potential of taking on any realistic configuration of parameters. At the same time, constraints on the synaptic parameters keep the resulting current within a range that is compatible with our somatic model (as defined in MacGregor and Oliver, 1974). The combination of these realistic parameters resulted in a model that approximates realistic neural function (Fig. 4).

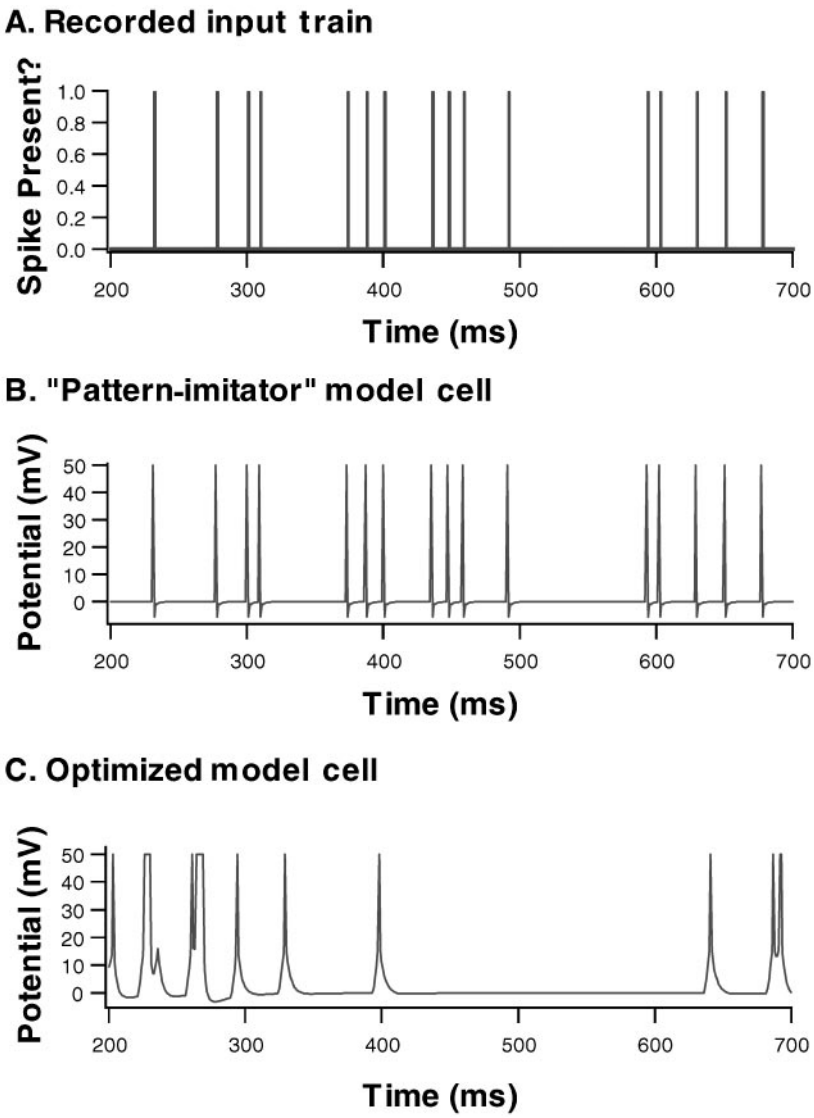

Figure 4. The realistic parameter ranges made for realistic firing behavior, which could be manipulated by modulating parameter settings. **A:** Recorded input trains are applied to the model. **B:** A cell that has been tuned to imitate the input in its output firing patterns. **C:** Response to the same input by a model cell with a different set of parameters optimized for further ISI discrimination. Note: Due to the time scale of the figure, spike bursts with short ISIs appear as broad action potentials.

2.4. Integration Method

The first-order differential equations listed above were integrated at millisecond intervals using an exponentially corrected Euler's method. MacGregor (1987) showed that this model has good stability with a 1 ms step size. As will be shown below (see Section 3, Results, Fig. 8), smaller step sizes did not alter the relationship between parameter choices and the model's performance.

2.5. Inputs to the Model

The purpose of the study was to generate model neurons, using the parameters described above, that would respond selectively to subranges of interspike intervals (ISIs). The inputs to these neurons were thus pairs of spike trains that were indistinguishable along all ISI ranges except for the subrange for which we wished selectivity (again, see Fig. 1). If a model neuron responded sufficiently differently to such a pair of spike

trains, we would know that it was responding to the ISI subrange where the differences resided.

All spike trains applied to the model were collected during a previous study (Bodnar and Bass, 1999), in which 514 recordings were elicited from the midbrain of 52 male midshipman. Each "pair of spike trains" that the model was asked to discriminate was acquired as follows:

- *Spike train 1* Two-tone stimuli, synthesized by custom software (CASSIE, designed by J. Vrieslander at Cornell University), were presented to the fish at naturally encountered frequencies. One tone was always 90 Hz, while the other differed from 90 Hz by + 2, 4, 6, 8, or 10 Hz. Ten trials of 1000 ms duration were recorded from a given midbrain cell to measure its response to these two tones.
- *Spike train 2* A second set of two-tone stimuli was also presented while making the same recording from the same cell. One of the tones was again set to 90 Hz. This time, however, while the second tone deviated from 90 Hz by the same amount as with spike train 1, it deviated in the opposite direction (this time by − 2, 4, 6, 8, or 10 Hz).

Consequently, while spike train 2 was gathered using the same amplitude, phase, and difference between the two tones, one of the tones was different from the one administered during the recording of spike train 1. The significant differences across subranges of ISIs observed between each pair of spike trains collected in this way (Bodnar and Bass, 1999) could thus be attributed to differences in frequency content. Asking the model to discriminate pairs of such spike trains was therefore equivalent to asking it to discriminate between the frequency information they contained.

The 514 pairs of spike trains recorded in this fashion were binned according to the high and low cutoffs of their differing ISI ranges. Spike-train pairs were considered similar enough to share a bin if both their high and low cutoffs differed by less than 5 milliseconds. A representative pair of recordings was selected from each of these bins and was applied to the model as an input.

An input to the model thus consisted of a pair of spike trains whose within beat ISI distributions diverged only over a specific ISI range. Altogether, we applied a full spectrum of ISI ranges encountered (see Section 3, Results, Fig. 7A), using tones that deviated across the entire natural range, for a total of 114 different ISI range inputs to the model.

2.6. Optimization of Modeled Cells

One modeled cell was generated and optimized to process each input. The goal of each cell was thus to take a pair of spike trains that only differed across a subrange of ISIs and produce an output pair of spike trains that differed across their entire range of within beat-period ISIs; as for the analysis of input spike trains, between beat-period ISIs were not included. For each inputed pair of spike trains, the parameters of a point neuron were varied until its overall response to one spike train in the pair was significantly different, in terms of overall ISI distribution, from its response to the other spike train in the input pair. Difference in distribution was measured by constructing ISI histograms for the model's two responses and performing a Mann-Whitney U-test ($Z > 1.95$, $p < .05$).

2.6.1. Brute-Force Method. Optimization on modeled cells was attempted by performing constrained minimization on the cell's 10-dimensional parameter space. Brute-force methods of trying random combinations of parameter settings immediately proved to be too coarse a strategy for localizing optimal parameter combinations. Therefore, and more efficient optimization routines were employed.

2.6.2. Downhill Simplex Method. The downhill simplex method, originally due to Nelder and Mead (1965), is an effective gradient-descent method for locating minima in multidimensional spaces. A simplex is a geometric figure comprising, in N dimensions, $N + 1$ points and the line segments and faces that connect them. Since each point of the simplex was a location in the parameter space that we hoped to minimize, points that evaluate to higher values represent worse performance. The simplex's mobile behavior was thus assigned several rules:

- When moving toward a local minimum, the point with the highest numerical evaluation (which represents the worst performance) is translated through the geometric center of the simplex. If this results in a combination of better performance (i.e., a lower evaluation function), the point remains. Otherwise it is returned to its original position.
- When all points evaluate to similar values (it appears to be on a "plain"), the simplex is expanded in search of a gradient.
- When sitting around the sides of a "valley," so that all good moves seem to be toward its interior, it

contracts around its center to locate a more precise minima.

The following rules were added to improve its performance:

- When stuck inside a long, narrow "gorge" in which movement in almost any direction results in worse performance, it locates the transverse direction of the gorge, if any, and proceeds quickly down it.
- When no such transverse direction exists, and it is reasonably sure that it has encountered a local minimum (the best point in the area but perhaps not in the entire parameter space), all points but the best one are relocalized to a random area of the search space and allowed to assume a stabilized form between its new points and the previous optimized one.
- After several runs of this procedure, the entire simplex is relocalized to a new region.

A successful implementation of the simplex method produced rapid minimization(Fig. 5), achieving in minutes what the brute-force method failed to achieve over days of computation. One limitation encountered with the simplex method was that since it searches by following a performance gradient, it always goes down while refusing to go up. Thus, it often gets stuck in tiny valleys, while a much deeper valley could reside just beyond. The topography was nonlinear in character, resulting in treacherous terrain. To overcome this problem, elements of simulated annealing (Kirkpatrick et al., 1983) were added to our simplex method to overcome the problem of local minima.

2.6.3. Simulated Annealing Method. Our implementation of simulated annealing modified step 1 above in the following way. As before, the translated point always remained if it resulted in a lower evaluation function; however, if it did not, it was allowed with probability p to remain despite this fact, whereas the move would have otherwise not been permitted. The value for p was initially set to 1 but was then gradually decreased to 0 as the search continued. This resulted in a gradient descent that would at first easily make upward moves but would become less likely to as time went on. The net result was that the searcher overcame large valleys first and then (through a slow reduction of p) began to settle in smaller and smaller valleys until it had found a close-to-global minimum region of the search space. We used simulated annealing to locate high-performance areas of the parameter space and then searched these spaces thoroughly through multiple runs of the downhill simplex method.

2.7. Computational Materials

Simulation, searching, and visualization software was custom-designed in C, with integrated analysis scripts written for MatLab (MathWorks, Inc.). Preliminary computation was performed on an IBM RS6000, with most of the parameter searching carried out on the IBM SP2 supercomputer at the Cornell Theory Center.

3. Results

We attempted to produce model neurons that responded selectively to specific ranges of interspike intervals (as discussed in Fig. 1). Through our optimization routines, we were able to develop neurons that preferred to respond to a subrange of ISIs, so that two inputs differing along that range would be significantly discriminated (Fig. 6). Figures 6A and 6B show interspike interval histograms of an example input spike train pair, while Figs. 6C and 6D show the corresponding interspike interval histograms for the model's output. The within beat ISIs are those which are less than approximately 100 ms, while the longer ISIs (peak near 150 ms) correspond to between beat ISIs. Qualitative differences can be observed in these probability distributions at shorter ISIs; however, it is difficult to determine the range and extent of these differences. The points of divergence in these ISIs are more easily observed in the inverse cumulative distributions (Figs. 6E and 6F). The plots in Fig. 6E show the inverse cumulative ISI distributions for the input spike train pair shown in A and B with the arrows designating the range of significantly different ISIs; a expanded view of this range is shown in the inset plot. The inverse cumulative distributions of the model output spike train pair are shown in Fig. 6F. The output spike trains differ from one another across their entire within beat ISI distributions ($\sim$ <100 ms) in the same manner as the subrange of the input spike trains.

Overall, 114 inputs were applied to the model (Fig. 7A). Most inputs (72%) consisted of a pair of spike trains that differed only across a narrow ISI range and were otherwise not significantly distinguishable (Fig. 7B). For each of these inputs, a point neuron was constructed that successfully discriminated between

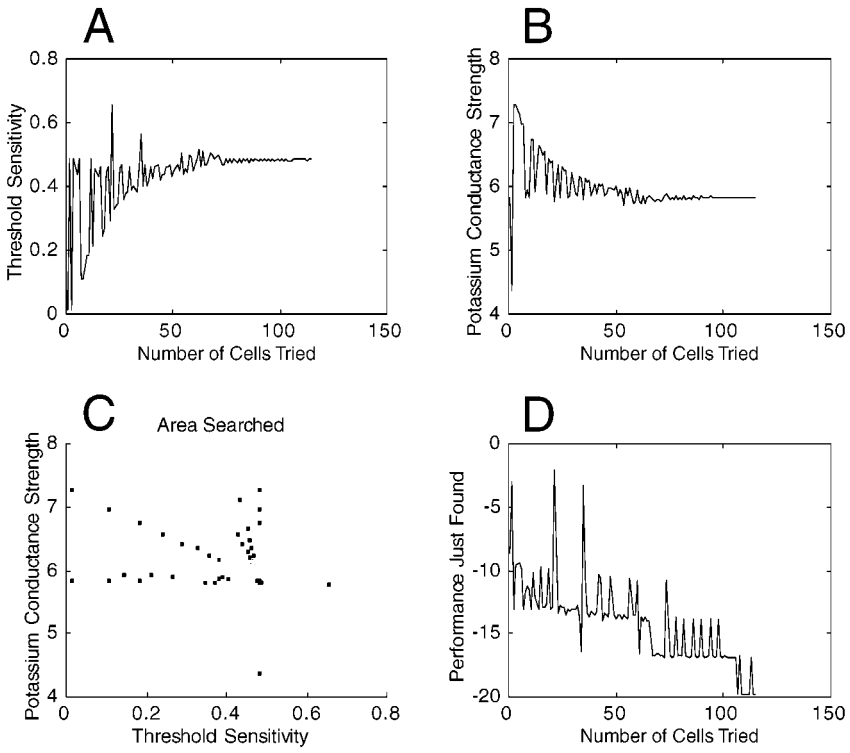

Figure 5. Examples of the convergence of parameter searching. Threshold sensitivity (**A**) and potassium conductance strength (**B**) quickly converge in their settings, as a solution is approached. **C:** Solution is found as searcher descends into areas of better performance. **D:** Meanwhile, performance found is rapidly optimized.

the two spike trains (Fig. 7C). The integration time step for our model did not influence the success of the neurons' discrimination. As shown in Fig. 8, reducing the time step by a factor of 10 did little to change the general behavior of our model. Thus, of the 114 ISI ranges applied, our model neurons processed 100% of them.

3.1. Properties of Modeled Cells

The model cells that resolved each input were not a collection of random solutions that happened to work in isolated instances. Rather, they had a great deal in common, implying a set of properties that universally facilitated the task. Most remarkably, all cells that successfully processed the inputs were exactly the same with respect to 8 of their 10 parameters. The parameter settings used in the model are marked in Fig. 9. This figure also depicts the effect, on average performance, of manually varying the parameters away from these optimal values. Performance generally decreased by varying individual parameters away from observed optimal values. The extent of this decrease, however, varied from one parameter to the next and exhibited a nonlinear character.

This nonlinearity is further emphasized when two parameters are varied together, as in Fig. 10. As can be seen, the effect of varying one parameter on performance depended on the particular setting of the other parameter. This illustrates the complexity of this optimizaton problem, as all 10 parameters had to be searched simultaneously.

Somatic properties that proved conducive to discrimination across all inputs included a medium-level initial threshold, a low membrane time constant, a high threshold time constant, and a high potassium conductance time constant.

While discriminating any ISI range required the careful selection of 8 universal parameters, selecting between the different ISI ranges was achieved by varying the remaining two parameters—threshold sensitivity and potassium conductance strength. These parameters were deemed likely candidates for extending

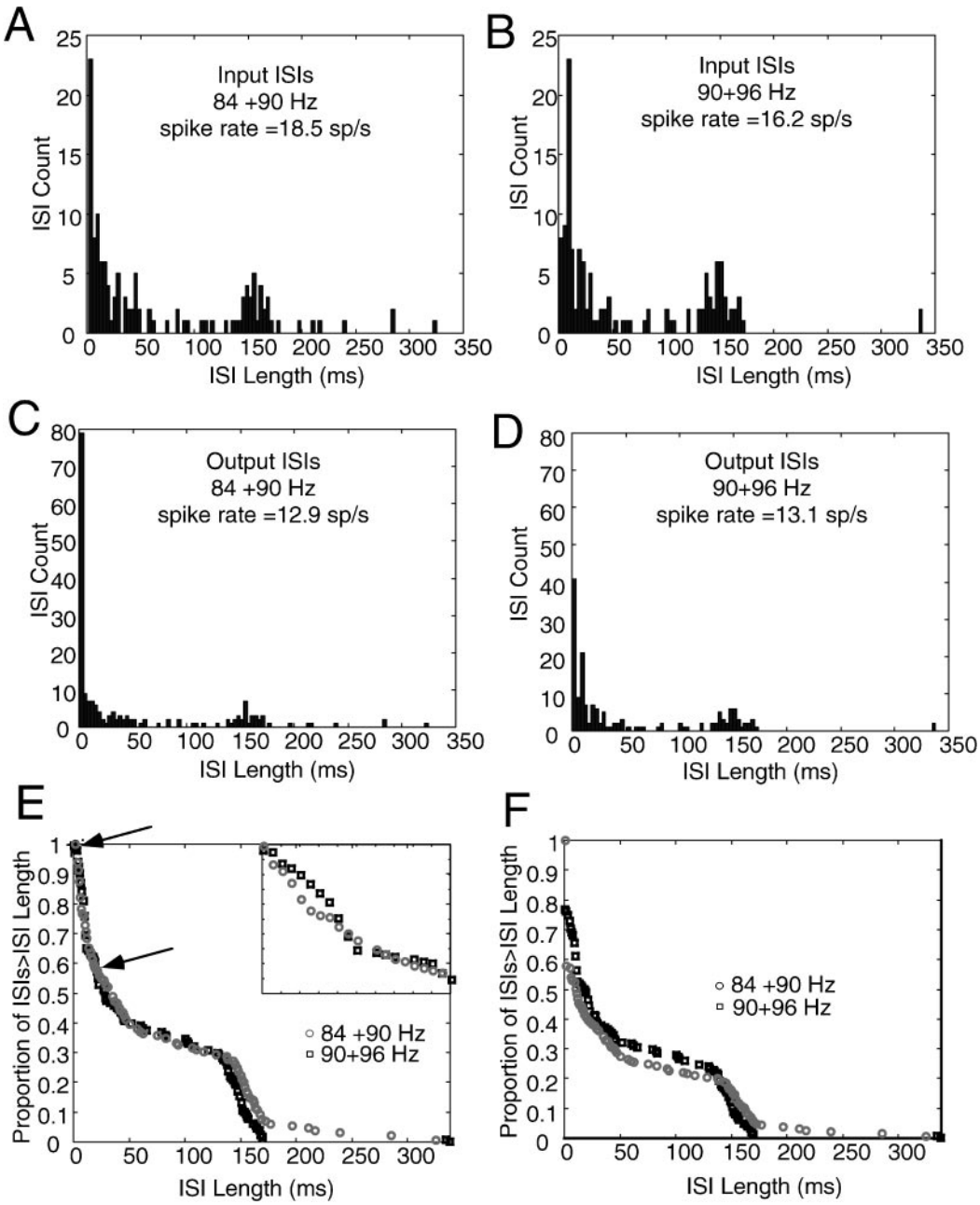

Figure 6. An example of the model's performance for a single pair of inputs. The model discriminates input patterns through the selective filtering of specific ISI ranges. **A, B:** Histograms of interspike intervals observed in two spike trains that were applied to the model; A: 84 + 90 Hz, B: 90 + 96 Hz. **E:** Cumulative ISI distributions same input spike trains from A and B. The arrows indicate range of statistical difference; an expanded view of this range is shown in the inset. **F:** Cumulative ISI distributions same model spike trains from C and D.

the range of discrimination through the type of information portrayed in Fig. 11. Each parameter was incrementally varied while monitoring its effects on the discrimination of each individual ISI range. Some parameters, such as synaptic input strength, exhibited wide ranges of settings in which no ISI ranges were discriminated well. For example, Fig. 11A demonstrates what happens to discrimination performance as the

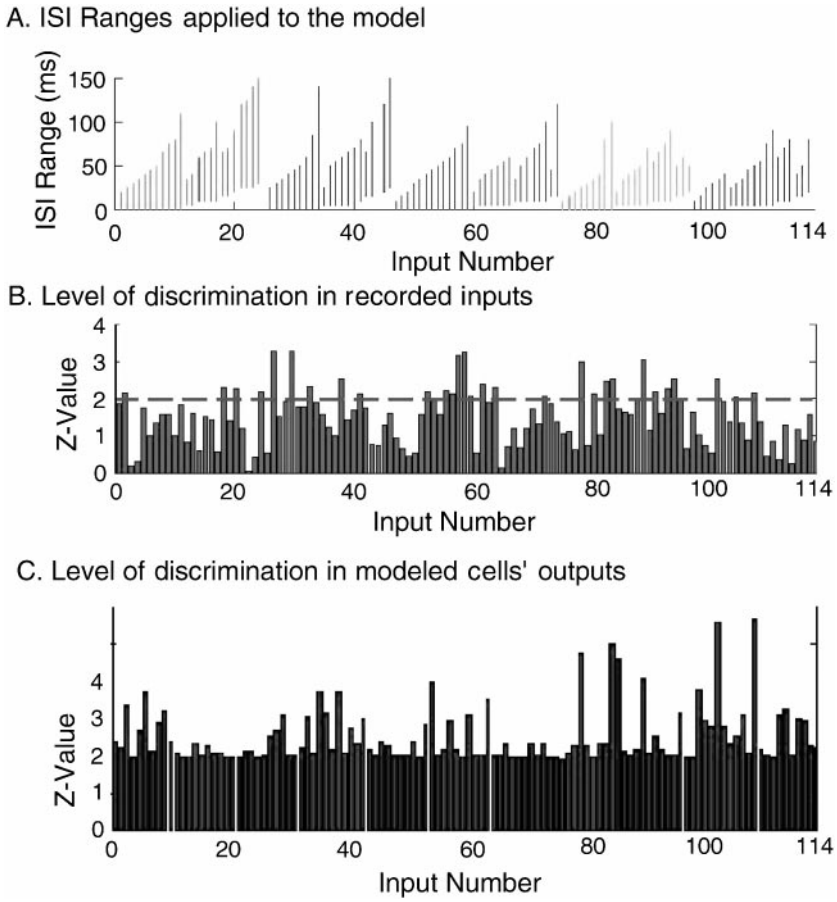

Figure 7. Model performance across all inputs. **A:** The model was asked to discriminate 114 pairs of spike trains, which encoded a complete spectrum of naturally-occurring pure tones, and with each's content differing along a unique ISI range. **B:** In most cases of the input, the overall information content between each pair of spike trains did not differ significantly ($Z < 1.95$; $p > .05$), as delineated by the dashed line. Nonetheless, in response to each such pair of inputs, the model generated a pair of output trains that contained significant differences in content **C:** 100% of the inputs were discriminated beyond significant levels ($Z > 1.95$; $p < .05$).

input current scale parameter is smoothly varied from its low value to its high value. At low values all ISI ranges are poorly discriminated, as denoted by the light hues. As the parameter setting approaches middle values, the hues quickly darken, indicating that the middle range provides good discrimination. As settings begin to get high, however, lighter hues are soon observed as discrimination worsens. Discrimination thus occurs over a restricted band of certain parameter settings, and this band is shared by most of the inputs. It made sense to set parameters exhibiting this pattern to the narrow range in which they conferred maximal discrimination.

A second type of pattern was exhibited by parameters like threshold sensitivity and potassium conductance strength. For these parameters, there was no clear setting that provided universal discrimination. Instead, moving the setting changed the selectivity of the cell from one group of ISI ranges to another. Figures 11B and 11C provide a graphical description of this effect. At low ranges of a parameter setting, certain ISI ranges are discriminated well (darker regions) while others are not (lighter regions). When shifting the parameter setting into the high range, however, these darker regions become light, and other ISI ranges that were previously marked with a light hue become darker. In cases like these, there was no globally optimal parameter setting: some settings worked for some ISI ranges, while another setting was needed for others. It was thus theorized that modulating these parameters might bring discrimination to even more ISI ranges

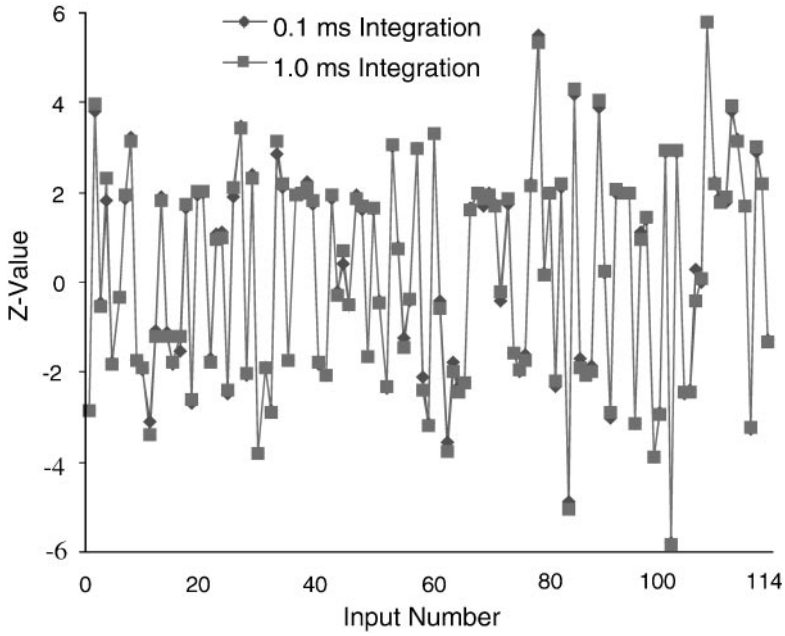

Figure 8. Model performance at a smaller time step size. Our findings were robust even when a smaller integration step size was applied to the model. When the step size is decreased by a factor of 10, from 1 ms to 0.1 ms, modeled neurons perform just as well at discriminating input patterns at significant levels.

than could be handled by a generally effective point neuron.

Admittedly there were several parameters that fit this criterion (such parameters are depicted in Fig. 9 by a relatively flat line). However, in the interest of keeping modeled cells as similar as possible, we attempted to minimize the parameters that could vary freely between cells. Two of the parameters differed from the other three in that their globally successful setting (midline of their Fig. 9 plot) was not their maximum setting, a fact that permitted more flexibility in the direction they could be potentially adjusted. These same two parameters had the additional property that they were not coupled: they did not define the same state variable (threshold time constant and threshold sensitivity were part of the same update equation and thus would not provide the same flexibility as two variables participating in two different equations). Given these standards and with all other factors seeming equal, these two parameters, threshold sensitivity and potassium conductance strength, seemed the most useful parameters to vary. Using this strategy to direct our optimization methods, we discovered that selectivity to all ISI ranges could be achieved by our realistic point neuron by ranging only two of its 10 parameters.

3.2. Observations of Modeled Cells' Behavior

Comparison of the firing activity between the model's input and output reveals some of its most interesting characteristics (Fig. 12). First, the output firing rate by all modeled cells is nearly identical to the firing rate of the recorded inputs (Fig. 12A: −dF spike trains; Fig. 12B: +dF spike trains). While the model seems to preserve spike rate, however, an examination of its firing patterns reveals that it is nonetheless exerting some form of selectivity (Fig. 12C). Only a fraction of the input spikes elicited a response from the modeled cells, which ignored an average of 25 out of 45 spikes (56%) every second.

Scrutinizing the model's firing patterns reveals the mechanism by which it is able to ignore certain spikes while still firing the same number of times (Fig. 13). Specifically, 25% of the model's output spikes were burst-like spike pairs with an ISI of 1 ms (Fig. 13A; example spike train in Fig. 4C). Figure 13B shows the distributions of all input ISIs, and Fig. 13C does the same for the output. When the disproportion of 1 ms ISIs is disregarded (Fig. 13D), it is observed that the output distribution closely resembles the input.

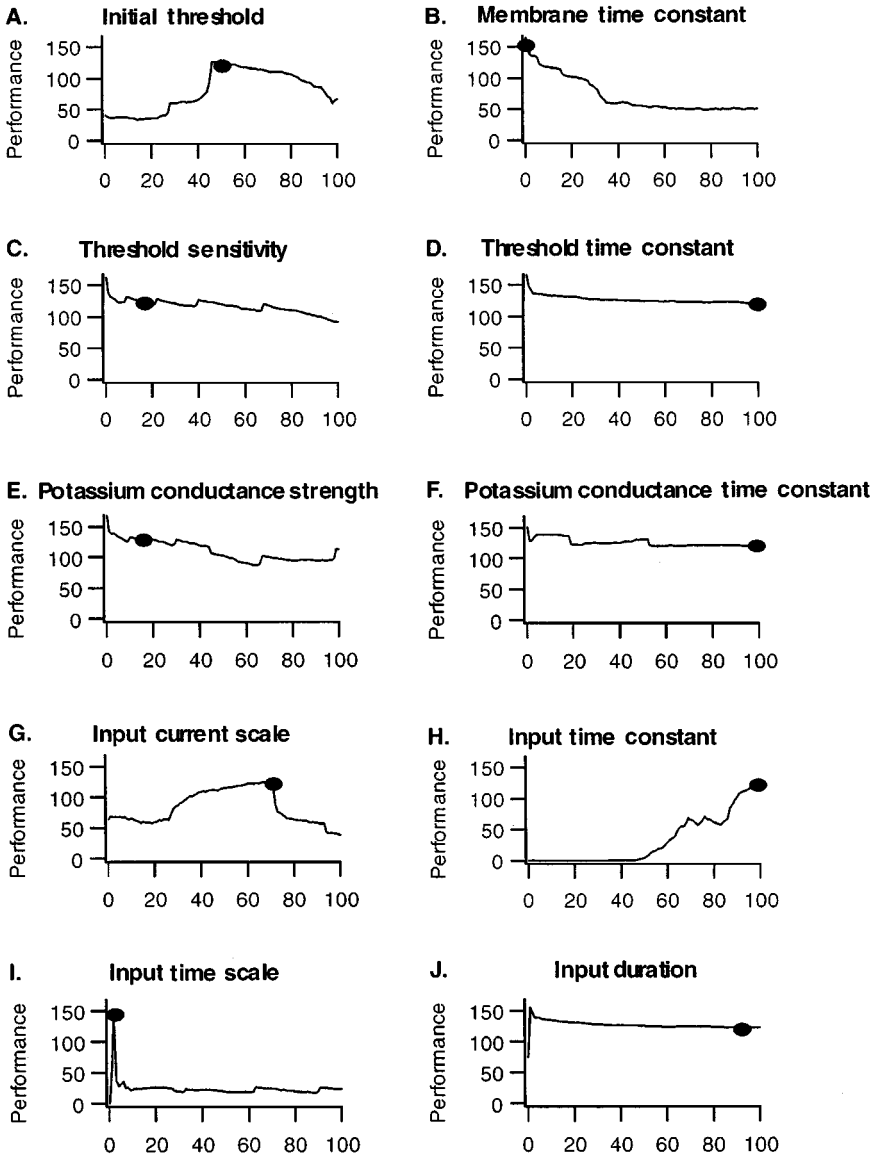

Figure 9. Each parameter setting is varied individually while the resulting change in the model's performance, summed across all inputs, is assessed. Each parameter was varied (X-axes) across its complete physiological range. Each parameter setting that contributed to the global minimum is marked with an oval. Some parameters (initial threshold, membrane time constant) seemed to demonstrate distinctly optimal settings. Others (threshold sensitivity, potassium conductance strength) did not show a clear maximal performance at any particular setting.

4. Discussion

Modeled cells, which were identical in all but two parameter settings, succeeded in extracting information from all midbrain-generated ISI ranges (Fig. 7). An examination into the interplay of the modeled set of parameters may yield a deeper understanding of the extraction algorithm and potentially insight into the encoding process as well.

4.1. Temporal Coding Versus Temporal Encoding

A fundamental issue in neural coding is how sensory stimuli are encoded within a spike train—via the

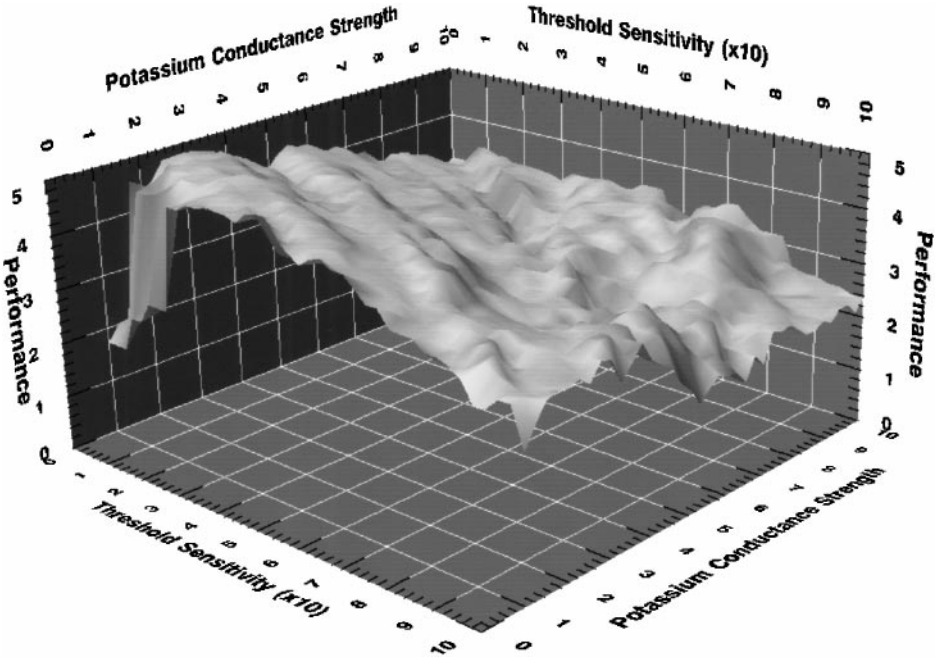

Figure 10. Two parameters (threshold sensitivity and potassium conductance strength) are varied in tandem while the resulting overall performance across all inputs is assessed. Color denotes the local slope of the surface at each given point to emphasize the curvature of the topography. The effect that varying one parameter has on performance changes depending on the particular setting of the other parameter, a nonlinearity that is further augmented when all 10 dimensions of the parameter space are considered simultaneously.

average spike number (rate coding)—by synchronization (temporal coding) or through the various timing patterns of the spikes (temporal encoding). Here we examine the representation of frequency information in the auditory midbrain of fish, which seems a poor example of temporal coding (Bodnar and Bass, 1997) but a possible candidate for temporal encoding (Bodnar and Bass, 1999) through representations across narrow ranges of interspike intervals. But its eligibility as a code depends on the feasibility of its decoding.

Analysis of frequency information on the basis of interspike intervals within the auditory CNS was first proposed by Licklider (1951, 1956). Under this model, frequency information is extracted by neural circuits that essentially perform an autocorrelation analysis via delay lines and coincidence detection, thereby filtering different ranges of interspike intervals. Our model demonstrates that interspike interval filtering can be achieved by a single point neuron and that variation of cellular parameters can determine the band-pass range of the interspike intervals.

The decoding of interspike intervals does not require anything more complex than neurons that are sensitive to the durations of individual ISIs, with some variability in the range of their response. Buonomano (2000) purports that this sensitivity can be embodied in a single synapse. The seeming complexity of such a code is offset by the potential simplicity of its implementation: it would not require averaging across stimulus repeats, stretches of time that may be long compared with the time scale of firing-rate modulation or a large population of neurons that carry similar information. This renders ISI processing equivalently feasible to more accepted representation forms such as rate coding. The success of our model in manipulating ISI distributions shows that this realm of processing may be more tenable than previously believed.

4.2. Analysis of Model's Output

Our model cells showed clear preference for certain spikes (Fig. 12C), while maintaining a spike rate strikingly comparable to that in their input (Figs. 12A and 12B). This was accomplished largely by making more spikes per response, through two-spike bursts that were markedly prevalent in the model

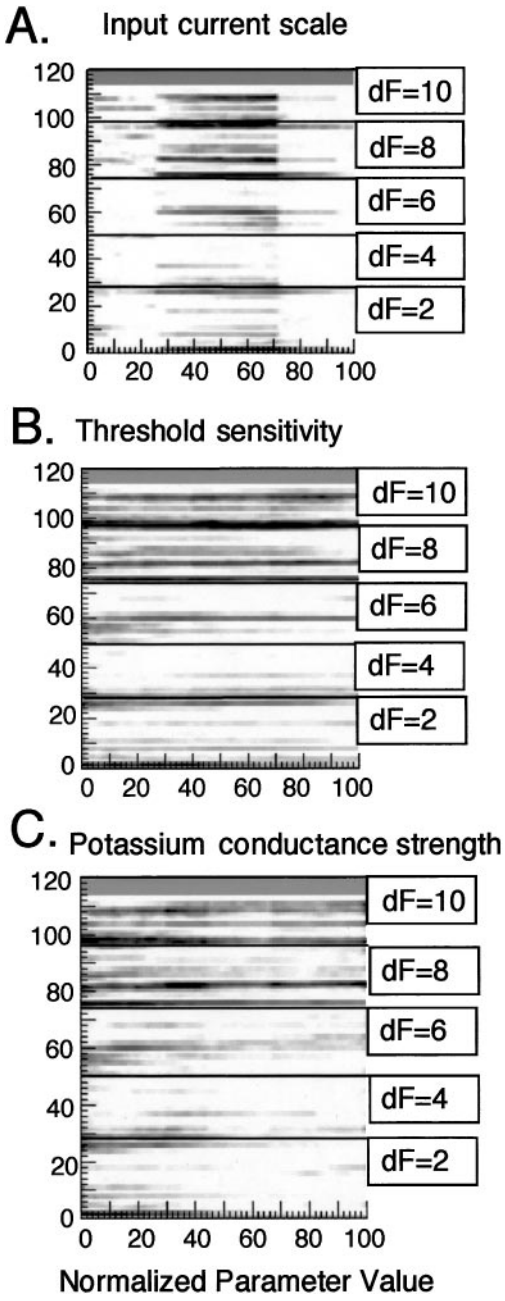

Figure 11. The model's performance on each individual input is assessed while single parameters are varied. With some parameters such as input current scale (**A**), a clear range of settings (30–70) provided good discrimination for many inputs, as denoted by the darker hues, while settings outside that range provided poor discrimination, as indicated by the lighter hues (inputs in A grouped by dF). With other parameters, such as threshold sensitivity (**B**) and potassium conductance strength (**C**), settings provided good discrimination of some inputs but not for others. As various inputs required various settings for optimal discrimination, it proved wise to permit flexibility in these parameters.

neuron outputs (Figs. 13A and 13C). Hence, the interspike intervals that were discriminated seemed to be bordered by not one but two spikes on a side. This would provide a statistically robust code, in that two spikes would have to be deleted in order for the duration of the longer interspike intervals to be significantly altered. In addition, given the large number of doublet spikes, many single spikes would have

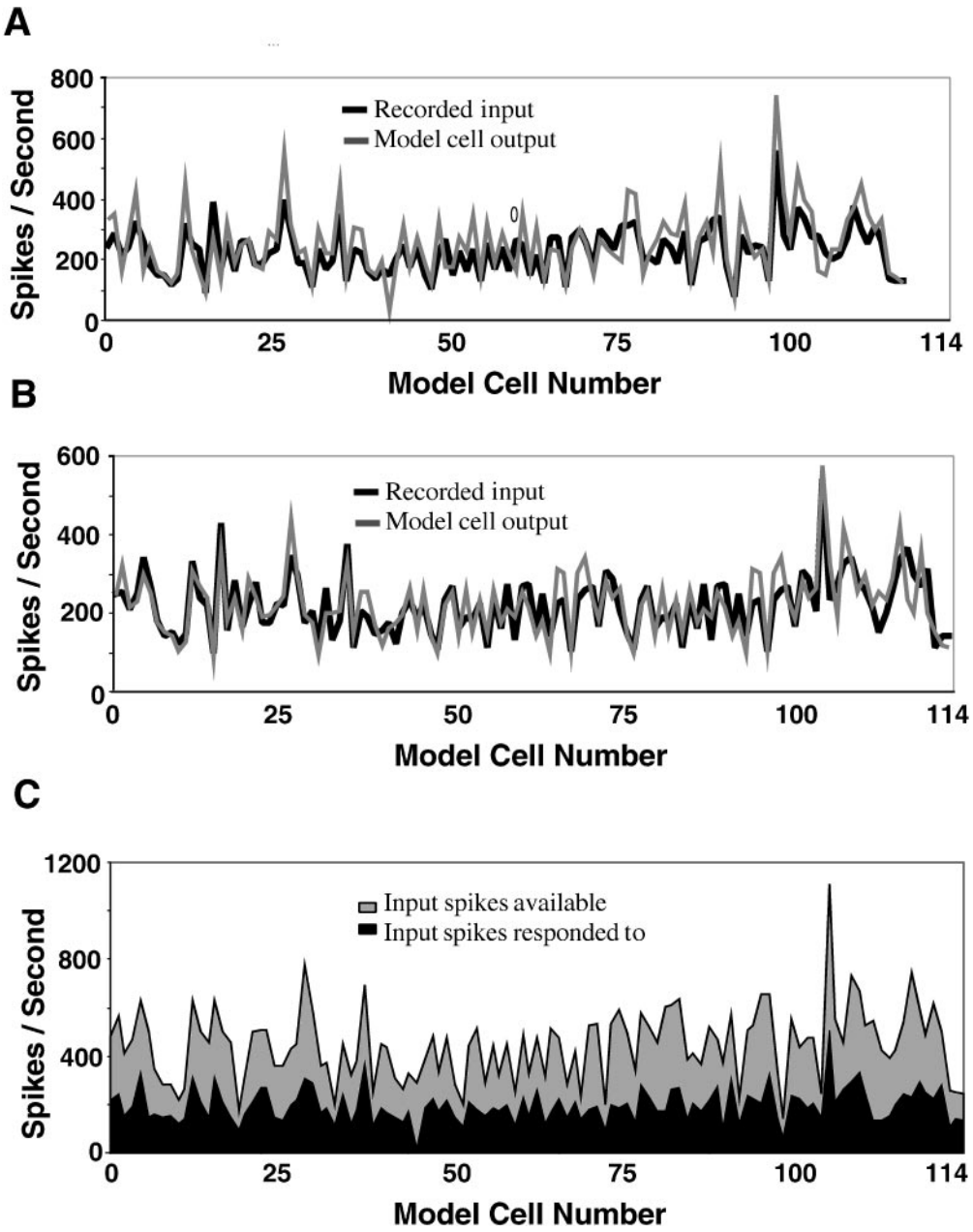

Figure 12. Spike-train properties of the modeled cells' output compared to their input. **A, B:** All 114 modeled cells preserved the overall rate of firing received in the input (A: −dF spike trains; B: +dF spike trains). **C:** All modeled cells also ignored a large percentage of available input spikes, indicating some form of selectivity.

to be lost to significantly reduce the number of short intervals.

The fact that all cells optimized exhibited these same firing properties suggests that they may be a basic feature of this extraction process, even across multiple ISI ranges. This transformation in the temporal characteristics of the spike-train code enhanced differences in the overall distribution of their interspike intervals elicited by different frequency content. Thus, our model demonstrates that modification of the temporal characteristics of a spike train alone, with no change to its average firing frequency, can greatly improve

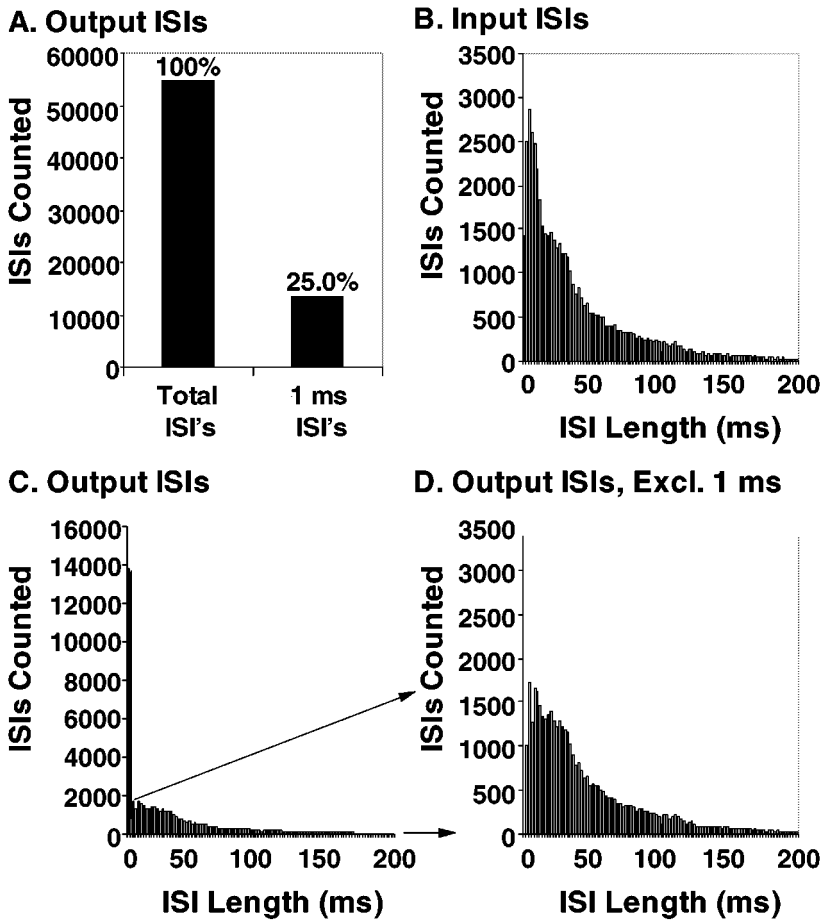

Figure 13. Comparison of input and output ISI distributions. **A:** 25% of all output ISI's were 1 ms in length, indicating bursting activity. **B:** A histogram of ISIs found in all input spike trains. **C:** A histogram of ISI's found in all output spike trains. **D:** A closer look at the nonbursting part of the output (excluding 1 ms ISIs).

discrimination between two spike trains and thereby the stimuli they encode.

4.3. Examination of Parameter Settings

Point neurons achieved successful discrimination across all inputs due to eight parameter settings that were universal amongst the modeled cells and two that were varied to accommodate specific inputs. As shown in Fig. 11, some parameter settings provided universal discrimination when locked within a narrow range (Fig. 11A), while others needed to be allowed to vary to cover the specific input in question (Figs. 11B and 11C).

Analysis of the mechanisms behind the parameters that needed to be varied may provide insight into why they could not be locked at a setting to provide universal discrimination. One of these parameters, threshold sensitivity, is a property of accommodation, while the other, potassium, conductance strength influences rectification.

Accommodation results in a less excitable membrane and occurs as a result of stimulation. The threshold sensitivity determines how quickly the cell becomes less excitable. A high value would cause the cell to become less excitable very soon after an impulse, thus leading the cell to ignore short intervals. A low value, in contrast, would permit small ISIs to be transduced, as only the shortest intervals in quick succession would render the cell inexcitable. A neural mechanism by which the threshold sensitivity could modulate discrimination was observed (Fig. 14). A

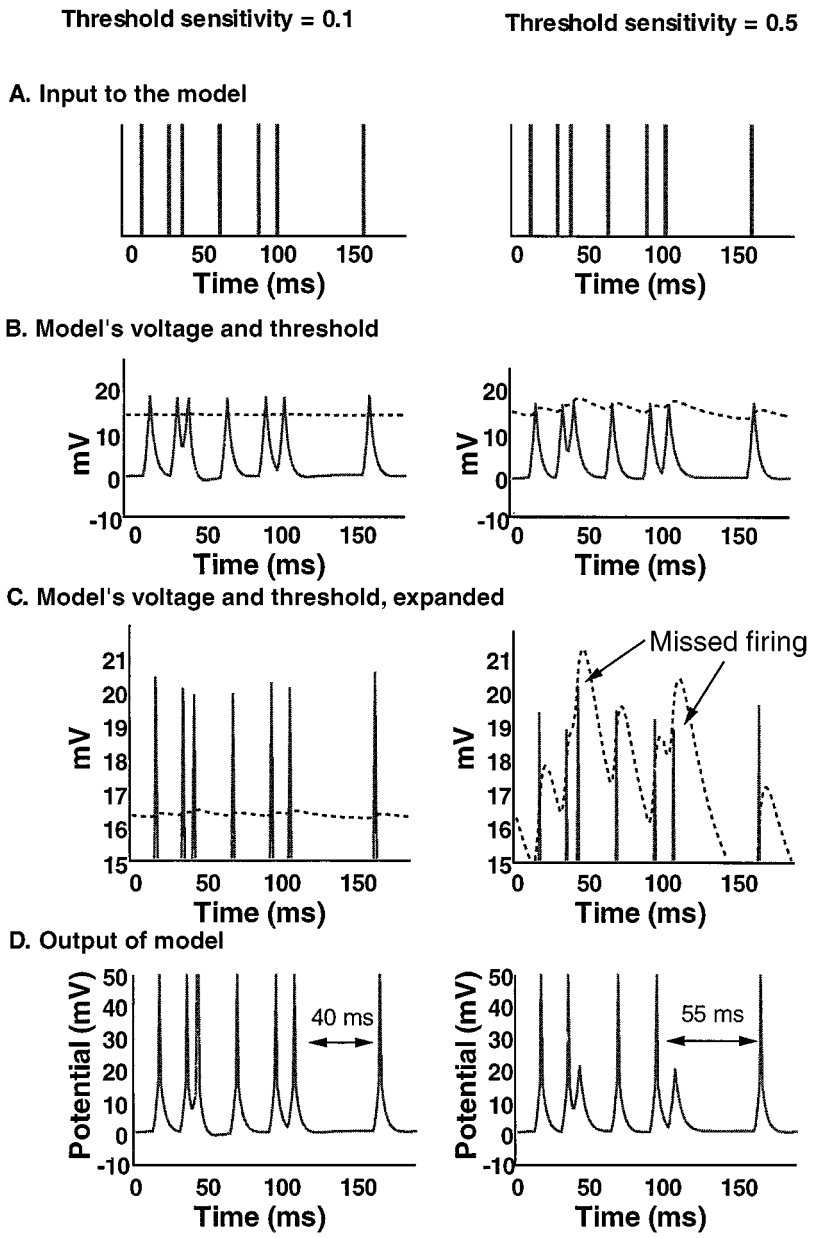

Figure 14. Modulating threshold sensitivity affects the resulting ISI distribution. **A:** Two different parameter settings (0.1, left; 0.5, right) confer thresholds with different sensitivities. **B:** Due to these different sensitivities, one threshold (right) fluctuates much more. **C:** These fluctuations allow the threshold to soar above the reach of some membrane excitation that would otherwise trigger action potentials. **D:** Thus, certain spikes that are present in the output on the left, are absent on the right. With spikes missing, ISI's measured (double arrows) are different.

sensitive threshold elevated more quickly than its rigid counterpart, so that the former cell failed to respond to the subsequent spike. With this spike missing from its output train, two shorter ISIs were converted into one longer one. This clearly has direct implications for the ISI distributions in the cell's output and consequently our assessment of discrimination ability.

We also examined how the potassium conductance strength modulated ISI distribution (Fig. 15). Rectification properties determine how quickly the

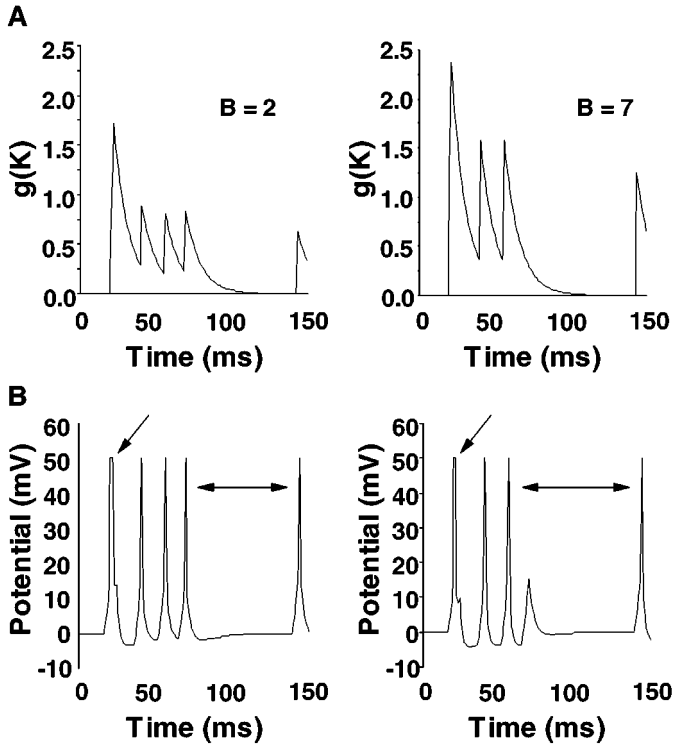

Figure 15. Modulating the potassium conductance strength affects the resulting ISI distribution. **A:** A higher setting for B results in a larger potassium conductance (right side). **B:** The increased potassium flow shortens what is a long burst (left side, first arrow) to a smaller burst (right side, first arrow). Note: Due to the time scale of the figure, 1 ms ISI bursts appear as broad action potentials. Additionally, the rectification completely inhibits one of the spikes, altering the ISI recorded (double arrows).

cell's membrane potential is repolarized from excitation and how long it remains in afterhyperpolarization. We noted that a cell with a higher setting for this parameter missed out on several firing opportunities. First, a higher potassium conductance strength (15A) causes a larger influx of potassium than a lower setting (15B). When a cell with this higher setting fires a burst of spikes, the resulting rectification is more powerful, and the burst ends one spike more abruptly than its low-setting counterpart. Consequently, a spike is missed and the ISI distribution is affected. Another result of a high setting was seen when a spike that one cell responded to was missed by the high-setting cell, which was still hyperpolarized when the input spike arrived. Again, a spike is missed, and the ISI distribution is modified. Varying only these two parameters produced modeled cells that varied enough to successfully process all of the inputs. It seemed necessary that the pair encompass two distinct aspects of the cell's current dynamics, in this case accommodation and rectification. Varying two parameters that defined the same current dynamic would probably not produce as wide a range of possibilities as varying two parameters that defined two different current dynamics.

4.4. Implications of the Model

The general view of neural coding by the midbrain is that frequency is encoded according to a rate-place code. Within the auditory system of mammals there is a tonotopic representation of frequency based on narrow spike rate tuning curves (Merzenich and Reid, 1974; Semple and Aitkin, 1979; Schriener and Langner, 1994). The segregation of concurrent vocal signals with small frequency differences poses a significant challenge to this coding strategy as the two frequencies will fall within the filter bandwidth and hence remain unresolved. In the midshipman, this coding strategy is even less likely as no tonotopic map has been identified in the midbrain and frequency tuning curves are not as narrowly tuned as mammals. Yet behavioral experiments have demonstrated that

midshipman are capable of segregating overlapping signals
with small dFs and hence, the central auditory system must encode frequency information in some form (McKibben and Bass, 1998).

In the peripheral auditory of midshipman as in other fishes, frequency is largely coded temporally via afferent synchronization (Fay, 1995; McKibben and Bass, 1999). In response to beats, midshipman afferents temporally code both components of the signal and show low synchronization to dF (McKibben and Bass, in review). Within the auditory midbrain, neurons show insignificant synchronization to the individual components of beats (Bodnar and Bass, 1997). However, differences in interspike intervals within specific ranges have been identified that potentially encode frequency information of beats (Bodnar and Bass, 1999). Our model demonstrates that these interspike interval patterns can be successfully discriminated. The model therefore provides an existence proof for how frequency information could be maintained in the higher auditory centers of the fish in the absence of a temporal synchronization code, potentially facilitating the segregation of concurrent vocal signals.

In midshipman frequency information appears to be transformed from a temporal code of absolute frequency in the periphery into an interspike interval code within the midbrain. The output of our model further tranforms the spike trains. How the midbrain interspike intervals represent frequncy remains unclear and is currently under investigation; there does not appear to be a simple mapping of frequency period onto the interspike intervals (Bodnar and Bass, unpublished observations). Hence, understanding how the model represents frequency information also remains undetermined. However, the performance of the model indicates that frequency information can be discriminated and hence is encoded within the spike trains. Determining the nature of the code both within the midbrain and postsynpatic neurons is the next step in understanding mechanisms involved in concurrent vocal signal segregation.

An alternate explanation for how frequency information could be propagated beyond primary nuclei as demonstrated here may provide insights into auditory processing by higher auditory centers in other vertebrates. Similar to midshipman, afferents in the mammalian auditory system temporally code the fundamental frequencies of concurrent vocal signals via synchronization to the individual components (Palmer, 1990; Cariani and Delgutte, 1996). Synchronization is maintained into the cochlear nucleus by at least two populations of neurons (Keilson et al., 1997). Within the auditory midbrain temporal coding of frequency information is not apparent; however, recent studies into the regularity of interspike intervals have been observed suggesting that temporal encoding may be present (Rees et al., 1997).

Alternate explanations, such as the temporal encoding examined here, require that normal cells can actually perform the computations necessary to discern them. The fact that the model achieves this computation, even through highly simplified cells constrained by natural physiology, strengthens the notion that such a decoding may in fact be possible. Specific predictions pertaining to the model are as follows. First the model predicts that discrimination will be carried out by cells of an average threshold that adapts slowly, a membrane that responds quickly, and a slow potassium conductance. Then just as the auditory periphery contains an array of cells tuned to narrow ranges of frequencies, the level of processing presented here predicts a bank of neurons selective for narrow bands of ISIs. Finally, locations for cells that could receive midbrain firing are anticipated by recently elucidated downstream connections of the nucleus centralis, the auditory center of the midshipman midbrain, and the homologue of the mammalian inferior colliculus. The level of processing discussed here most likely takes place in one or more of the targets of the nucleus centralis, such as the medial pretoral, lateral preglomerulus, or central posterior nuclei (Bass et al., 2000).

Apart from predictions related to the system in question, the work presented here attempts to provide an example of using modeling to explore the feasibility of temporal encoding, while delineating its biological constraints. Further work uniting experiment with high-powered modeling will hopefully make the more complex forms of neural coding more accessible.

Acknowledgments

We are grateful to Dr. Andrew Bass for laboratory resources, as well as for offering a great deal of time in discussion to flush out the theoretical framework for the model. We also thank the Cornell Theory Center for generous computational resources and Margaret Marchaterre for logistical support. This research was supported by NIDCD Grant DC-00092 to Andrew

Bass. The Cornell Theory Center receives funding from Cornell University, New York State, Federal agencies and corporate partners.

References

Balis UJ, Morris KF, Koleski J, Lindsey BG (1994) Simulations of a ventrolateral medullary neural network for respiratory rhythmogenesis inferred from spike train cross-correlation. *Biol. Cybern.* 70:311–327.

Bass AH, Bodnar DA, Marchterre MA (2000) Midbrain acoustic circuitry in a vocalizing fish. *J. Comp. Neur.* 419:505–531.

Bodnar DA, Bass AH (1997) Temporal coding of concurrent acoustic signals in auditory midbrain. *J. Neurosci*.17:7553–7564.

Bodnar DA, Bass AH (1999) Midbrain combinatorial code for temporal and spectral information in concurrent acoustic signals. *J. Neurophys*. 81:213–232.

Brantely RK, Bass AH (1994) Alternative male spawning tactics and acoustic signals in the plainfin midshipman, *Porichthys notatus. Ethology* 96:213–232.

Buonomano DV (2000) Decoding temporal information: A model based on short-term synaptic plasticity. *J. Neurosci*. 20: 1129–1141.

Cariani P, Delgutte B (1996) Neural correlates of the pitch of complex tones. I. Pitch and pitch salience. *J. Neurophysiol*. 76:1698–1716.

Fay RR (1993) Structure and function in sound discrimination among vertebrates. In: Webster DB, ed. *The Evolutionary Biology of Hearing*. Springer, New York. pp. 229–266.

Fay RR (1995) Perception of spectrally and temporally complex sounds by the goldfish (*Carassius auratus*). *Hear. Res.* 89:146–154.

Ghazanfar AA, Stambaugh CR, Nicolelis MAL (2000) Encoding of tactile stimulus location by somatosensory thalamocortical ensembles. *J. Neurosci*. 20:3761–3775.

Ghoshal S, Kim DO, Northrop RB (1992) Amplitude-modulated tone encoding behavior of cochlear nucleus neurons: Modeling study. *Hear. Res*. 58:153–165.

Hill, AV (1936) Excitation and accommodation in nerve. *Proc. R. Soc. London, Ser. B*. 119:305–355.

Ibara RM, Penny LT, Ebeling AW, van Dykhuizen G, Cailliet G (1983) The mating call of the plainfin midshipman fish, *Porichthys notatus*. In: DGL Noakes, DG Lindquist, GS Helfman, JA Ward, eds. *Predators and Prey in Fish*. Junk Press, The Hague, Netherlands.

Jack JJ, Noble D, Tsien RW (1975) *Electrical Current Flow in Excitable Cells*. Clarendon Press, Oxford.

Keilson SE, Richards VM, Wyman BT, Young ED (1997) The representation of concurrent vowels in the cat anesthetized ventral cochlear nucleus: Evidence for a periodicity-tagged spectral representation. *J. Acoust. Soc. Am*. 102:1056–1071.

Kernell D (1968) The repetitive impulse discharge of a simple neuron model compared to that of spiral motoneurons. *Brain Res*. 11:685–687.

Kirkpatrick S, Gelatt CD, Vecchi MP (1983) Optimization by simulated annealing. *Science* 220:671–680.

Laurent G, Wehr M, Davidowitz H (1996) Temporal representations of odors in an olfactory network. *J. Neurosci*. 16:3837–3847.

Licklider JCR (1951) A duplex theory of pitch perception. *Experientia*. 7:128–134.

Licklider JCR (1956) Auditory frequency analysis. In: Cherry C, ed. *Information Theory, Third London Symposium*. Butterworths Scientific Publications, London. pp. 253–268.

MacGregor RJ (1987) *Neural and Brain Modeling*. Academic Press, San Diego.

MacGregor RJ, Oliver RM (1974) A model for repetitive firing in neurons. *Biol. Cybernet.* 40:113–126.

McClurkin JW, Optican LM, Richmond BJ, Gawne TJ (1991) Concurrent processing and complexity of temporally encoded neuronal messages in visual perception. *Science* 253:675–677.

McKibben JR, Bass AH (1998) Behavioral assessment of acoustic parameters relevant to signal recognition and preference in a vocal fish. *J. Acoust. Soc. Am*. 104:3520–3533.

McKibben JR, Bass AH (1999) Peripheral encoding of behaviorally relevant acoustic signals in a vocal fish: Signal tones. *J. Comp. Physiol. A*. 184:563–576.

McKibben JR, Bass AH (in review) Peripheral encoding of behaviorally relevant acoustic signals in a vocal fish: harmonic and beat stimuli. *J. Comp. Physiol.*

Merzenich MM, Reid MD (1974) Representation of the cochlea within the inferior colliculus of the cat. *Brain Res*. 77:397–415.

Middlebrooks JC, Clock AE, Xu L, Green DM (1994) A panoramic code for sound location by cortical neurons. *Science* 264:842–844.

Nelder JA, Mead R (1965) A simplex method for function minimization. *Computer J.* 8:308–313.

Palmer AR (1990) The representation of the spectra and fundamental frequency of steady-state single- and double-vowel sounds in the temporal discharge patterns of guinea pig cochlear nerve fibers. *J. Acoust. Soc. Am.* 88:1412–1426.

Popper AN, Fay RR (1993) Sound detection and processing by fish: Critical review and major research questions. *Brain Behav. Evol.* 41:14–38.

Reich DS, Mechler F, Purpura KP, Victor JD (2000) Inter-spike intervals, receptive fields, and information encoding in primary visual cortex. *J. Neurosci.* 20:1964–1974.

Rees A, Sarbaz A, Malimerica MS, LeBeau FEN (1997) Regularity of firing of neurons in the inferior colliculus. *J. Neurophysiol.* 77:2945–2965.

Richmond BJ, Optican LM, Spitzer H (1990) Temporal encoding of two-dimensional patterns by single units in primate visual cortex. I Stimulus-response relations. *J. Neurophysiol.* 64:351–368.

Schreiner CE, Langner G (1994) Laminar structure of frequency organization in auditory midbrain. *Nature* 388:383–386.

Semple MN, Aitkin LM (1979) Representation of sound frequency and laterality by units in the central nucleus of cat inferior colliculus. *J. Neurophsiol.* 42:1626–1639.

Theunissen F, Miller JP (1995) Temporal encoding in the nervous system: A rigorous definition. *J. Comput. Neurosci.* 2:149–162.

Wehr M, Laurent G (1996) Odour encoding by temporal sequences of firing in oscillating neural assemblies. *Nature* 384: 162–166.